Energy dispersive detector for white beam synchrotron x-ray fluorescence imaging

Matthew D. Wilson' , Thomas Connolley, Igor P. Dolbnya, Patrick S. Grant, Enzo Liotti, Andrew Lui, Andrew Malandain, Kawal Sawhney, Paul Seller, and Matthew C. Veale

Citation: AIP Conference Proceedings **1741**, 050008 (2016); doi: 10.1063/1.4952928
View online: http://dx.doi.org/10.1063/1.4952928
View Table of Contents: http://aip.scitation.org/toc/apc/1741/1
Published by the American Institute of Physics

Energy Dispersive Detector for White Beam Synchrotron X-ray Fluorescence Imaging

Matthew D. Wilson[1, a)], Thomas Connolley[2], Igor P. Dolbnya[3], Patrick S. Grant[4], Enzo Liotti[4], Andrew Lui[4], Andrew Malandain[3], Kawal Sawhney[3], Paul Seller[1] and Matthew C. Veale [1]

[1] *Science and Technology Facilities Council, Rutherford Appleton Laboratory, Harwell Campus,UK.*
[2]*Diamond Light Source, I12 Beamline, Harwell Campus, Didcot, Oxfordshire, UK.*
[3]*Diamond Light Source, B16 Beamline, Harwell Campus, Didcot, Oxfordshire, UK*
[4]*Department of Materials, University of Oxford Parks Road, Oxford, UK.*

[a)]*Corresponding author: Matt.Wilson@stfc.ac.uk*

Abstract. A novel, "single-shot" fluorescence imaging technique has been demonstrated on the B16 beamline at the Diamond Light Source synchrotron using the HEXITEC energy dispersive imaging detector. A custom made furnace with 200μm thick metal alloy samples was positioned in a white X-ray beam with a hole made in the furnace walls to allow the transmitted beam to be imaged with a conventional X-ray imaging camera consisting of a 500 μm thick single crystal LYSO scintillator, mirror and lens coupled to an AVT Manta G125B CCD sensor. The samples were positioned 45° to the incident beam to enable simultaneous transmission and fluorescence imaging. The HEXITEC detector was positioned at 90° to the sample with a 50μm pinhole 13cm from the sample and the detector positioned 2.3m from pinhole. The geometric magnification provided a field of view of 1.1x1.1mm^2 with one of the 80x80 pixels imaging an area equivalent to 13μm^2. Al-Cu alloys doped with Zr, Ag and Mo were imaged in transmission and fluorescence mode. The fluorescence images showed that the dopant metals could be simultaneously imaged with sufficient counts on all 80x80 pixels within 60s, with the X-ray flux limiting the fluorescence imaging rate. This technique demonstrated that it is possible to simultaneously image and identify multiple elements on a spatial resolution scale ~10μm or higher without the time consuming need to scan monochromatic energies or raster scan a focused beam of X-rays. Moving to high flux beamlines and using an array of detectors could improve the imaging speed of the technique with element specific imaging estimated to be on a 1s timescale.

INTRODUCTION

The ability to simultaneously image the distribution of elements throughout a sample, *in-situ* during an experiment with timing resolution is desirable in a number of fields, with metal alloy solidification used as an example in this case. X-ray transmission imaging techniques using metal alloy analogues or simple binary alloy models have been insightful studies but do not provide vital information on the elemental distribution in the liquid phase and cannot be used to simultaneously image many elements in the sample [1]. Conventional Synchrotron X-ray Fluorescence (SXRF) can provide detailed maps of the elemental composition by raster scanning a focused X-ray beam over a sample and measuring the fluorescence spectrum on a Ge or Si based detector with only a single or relatively small number of channels [2]. This can provide spatial resolution as low as 1μm but the scanning process prohibits time resolved experiments. Here, we use the HEXITEC energy resolving imaging detector [3] and a pin-hole projection to collect X-ray fluorescence images of a metal alloy sample that is flood illuminated with a white X-ray beam.

Proceedings of the 12th International Conference on Synchrotron Radiation Instrumentation – SRI2015
AIP Conf. Proc. 1741, 050008-1–050008-4; doi: 10.1063/1.4952928
Published by AIP Publishing. 978-0-7354-1398-6/$30.00

EXPERIMENTAL ARRANGEMENT

The experiments were conducted on the B16 Optics and Metrology Beamline at the Diamond Light Source, UK. A white beam from the bending magnet source with an area of 5x5mm^2 was used as the primary beam to illuminate a metal alloy sample. The 200µm thick, 10x20mm alloy was made from an Al-Cu matrix with Ag, Zr and Mo added to the sample. The alloy was held in a custom made furnace at 45° from the primary beam which heated the alloy in an Ar atmosphere. Conventional X-ray transmission radiographs were measured with a 500µm LYSO scintillator optically coupled to an AVG Manta G125B CCD camera via a 90° mirror 17.5cm behind the sample. The transmission camera provided at field of view (FoV) of 5mm x 3.8mm and each pixel imaged an area equivalent to 3.96µm x 3.96µm. The X-ray fluorescence image was measured with the HEXITEC detector positioned 90° to the primary beam. The fluorescence X-rays were projected through a 1mm W plate with a 50µm pinhole positioned 13cm from the sample and the HEXITEC detector was positioned 231cm from the pinhole. The 80x80 pixels on a 250µm pitch of the HEXITEC detector provided a FoV of 1.1mm x 1.1mm and each pixel measured an area of 13.75µm. The detector had a 1mm thick CdTe detector that was held at 20°C and biased at -500V and has previously been characterized with an average pixel energy resolution of 800eV FWHM at 60keV [3]. The detector operates at a frame rate of 9 kHz with a maximum detection rate of 10^5 photons/s whilst still being able to correct for charge sharing [4]. A He filled flight tube with a 50µm thick Kapton windows was placed between the pinhole and the HEXITEC detector to reduce the attenuation of the fluorescence X-rays. A schematic of the experimental arrangement is shown in Figure 1, not to scale.

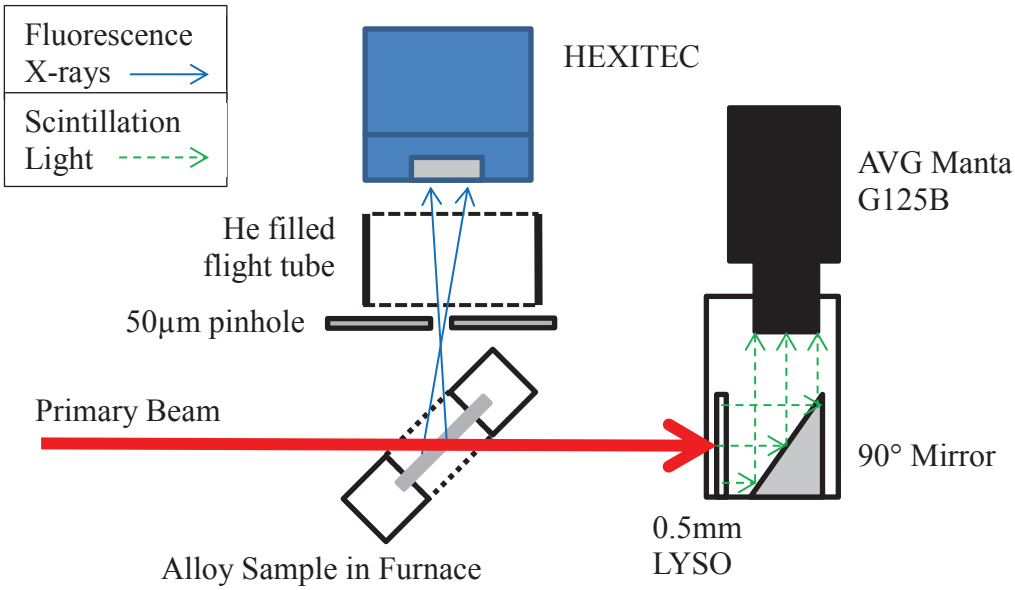

FIGURE 1. Schematic of the experimental arrangement, not to scale.

RESULTS

The experimental configuration was tested and aligned using a gold TEM grid (Gilder G200HS) that was 7.5 µm thick and had 125 µm pitch mesh, 12 µm bar width and 113 µm gaps. Figure 2 (a) shows the spectrum from 4x4 pixels in the region of the frame of the mesh (high intensity in Figure 2 (b)) were summed together to provide a spectrum with higher statistics. The Au L lines were visible between 9keV and 13keV. The characteristic Cd and Te K lines from 23keV to 31keV due to the self-fluorescence of the detector and fluorescence from the Lu at 53keV to 62keV in the LYSO scintillator were observed. As the TEM grid is increasingly transparent to the higher energy the K line from Au at had low intensities. Additional Pb shielding was added to prevent the Lu fluorescence from reaching the HEXITEC detector. This also meant that there were no X-rays above the K-edge of Cd or Te so their fluorescence lines were also removed from the spectra. Figure 2 (b) shows the number of counts per pixel when the

spectra per pixel were integrated from 9keV to 13keV to cover the L lines from Au. The image demonstrates that the configuration was able to resolve 125µm spaced features despite blurring from the 50µm pinhole.

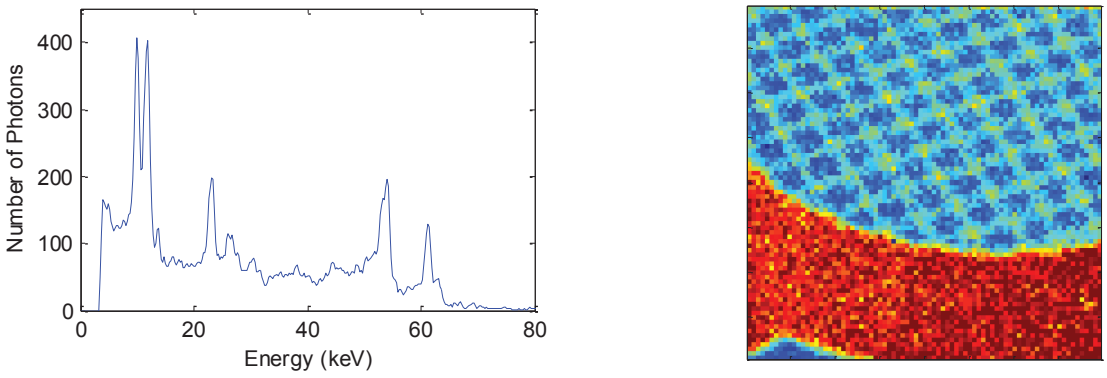

FIGURE 2. (a) A spectrum from 4x4 pixels on the mesh frame summed together with the Au L lines in. (b) An image of the intensity per pixel from 9keV to 13keV to cover the Au L line.

The sample was heated to 560°C and an image was collected in a region of the sample where there were Zr, Mo and Ag rich regions. Figure 3 (a) shows a section of the transmission radiograph collected with an integration time of 0.008s. Given the low flux of fluorescence X-rays the fluorescence data was collected for 60s. Figure 3 (b) shows the spectrum from 3x3 pixels summed together from regions of the image that were rich in Ag (blue), Mo (red) and Zr (black). The Cu from the Al-Cu matrix was not visible as the 8.0keV Cu K_α lines were heavily self-absorbed. The spectra per pixel were integrated over different energy ranges to provide images of the different elements. Images (c) to (e) had a median filter over a 3x3 pixel range applied to smooth the images. The Zr image in (c) was from the integration from 15keV to 16keV to cover the Zr K_α line only. The Mo image in (d) was from the integration from 17keV to 20keV to cover the K_α and K_β lines. As the K_β line from Zr is at 17.7keV and the Mo K_α line is at 17.5keV, they could not be separated and had to be corrected. The number of Zr K_α events was used to estimate the expected number of Zr K_β events [5], which were subtracted from the Mo image. This correction worked reasonably well but left some artefacts, for example in the bottom left hand corner of image (d). The Ag image in (e) was from the integration from 21keV to 25keV to cover the Ag K_α and K_β lines. This image and the spectra per pixel show that there were appreciable concentrations of Ag across the image due to the comparatively fast diffusion of Ag at this temperature, whereas the Zr and Mo were much slower to dissolve and diffuse at this temperature. Further details on the solidification experiments can be found in Liotti et al. [6].

DISCUSSION AND SUMMARY

This work has shown that the fluorescence imaging configuration with the energy discriminating imaging HEXITEC detector can image the elemental distribution of a sample with elements emitting fluorescence energies greater than 10keV. The spectrum per pixel provided suitable images in 60s exposures but this limitation was from the fluorescence flux which was < 200 photons per pixel per minute. The detector would be capable of collecting up to 1000 photons/pixel/s that would allow images to be collected in < 1s. High imaging rates could also be achieved by summing the spectra of neighboring pixels at the expense of spatial resolution.

The spatial resolution was limited by the pinhole projection onto the HEXITEC detector. This means that feature sizes of 10-20µm appear to be the resolution limit to the technique. Although this would be too large for some applications there are many areas, for example in material science, where this feature size or larger would be applicable. Additionally the combination of high resolution transmission imaging and lower resolution fluorescence imaging could be combined to provide new insight even if the fluorescence information is at a lower resolution.

The field of view of the HEXITEC detector at the highest magnification was only 1x1mm^2. HEXITEC detectors are butt-able on 3 sides and have been tiled in 2x2 [7] and 5x5 [8] detector modules with dead spaces of < 2 pixels between the individual detectors. This method of creating a large focal plane detector could be used to create a larger field of view for fluorescence imaging instruments in the future. Unlike the scanning techniques, adding more pixels to the detector would not slow the imaging rate whilst increasing the FoV.

Further optimization of experimental geometry and testing on the I12 Joint, Engineering, Environmental and Processing beamline at the Diamond Light Source are planned to demonstrate the potential at higher fluorescence energies and with a higher flux provided by the beamline. The suitability of imaging the elemental distribution on the 1-10s timescale with a spatial resolution on the order of 10μm or larger will be investigated with potential applications in metal alloy growth, geology, catalytic and chemical processing.

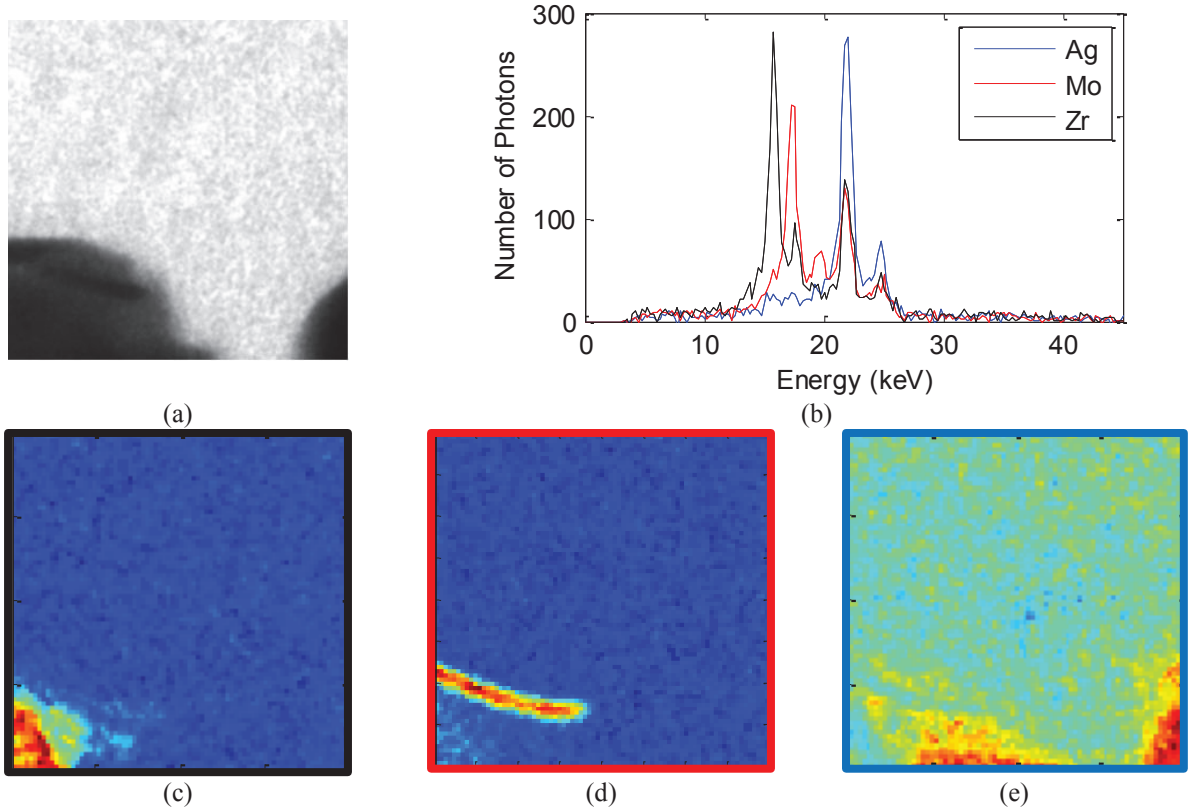

FIGURE 3. (a) The transmission radiograph image cropped and rotated to provide the same FoV as the fluorescence images. (b) The spectrum from 3x3 pixels summed together from areas that were Ag, Mo and Zr rich. (c) An image of the number of counts per pixel from the Zr K_α line only. (d) An image of the number of counts per pixel from the Mo K_α and K_β lines. (e) An image of the number of counts per pixel from the Ag K_α and K_β lines.

ACKNOWLEDGEMENTS

PG, AL and EL would like to thank the UK Engineering and Physical Sciences Research Council for financial support through grant EP/H026177/1.

REFERENCES

1. Mirihanage, W.U. et al., *Acta Materialia*, 81, pp.241–247. 2014.
2. V. M. Egerton, et al., J. Anal. At. Spectrom., 30, 627-634, 2015.
3. P. Seller, et al., JINST, 6, C12009, 2011, doi: 10.1088/1748-0221/6/12/C12009
4. M. Veale, et al., Nucl. Inst. Meth. A, 767, 218-226, 2014, doi:10.1016/j.nima.2014.08.036
5. A. Thompson, et al., "X-ray Data Booklet", LBNL/PUB-490 Rev. 3, 2009.
6. E. Liotti, et. al, submitted to Scientific Reports, June 2015
7. M. D. Wilson, et al., IEEE Trans. Nucl. Sci, 60, 2, 2013.
8. M. D. Wilson, et al., Submitted to J. Inst, June 2015.